POLITECNICO DI TORINO
Repository ISTITUZIONALE

Use of higher-order Legendre polynomials for multilayered plate elements with node-dependent kinematics

(Article begins on next page)

01 May 2024

Use of higher-order Legendre polynomials for multilayered plate elements with node-dependent kinematics

E. Carrera*, E. Zappino, A. Pagani, G. Li, A.G. de Miguel

MUL² Group, Department of Mechanical and Aerospace Engineering, Politecnico di Torino, Corso Duca degli Abruzzi 24, 10129 Torino, Italy.

Abstract

In the present work, higher-order Legendre polynomials are adopted as shape functions of p-version plate finite elements (FEs) and used in combination with node-dependent kinematics (NDK) to construct computationally efficient global-local FE models for the analysis of multilayered plates. The use of higher-order Legendre polynomials enables the elements to accommodate the complex structural deformations with a fewer number of variables in the FE model. Derived from Carrera Unified Formulation (CUF), NDK can integrate plate kinematics based on Equivalent Single Layer (ESL) models and Layer-wise (LW) models to obtain global-local models using no *ad hoc* coupling. The combination of Legendre-type shape functions and NDK shows excellent rates of convergence, which can lead to FE model with high accuracy in the refined local area with a reduction in the computational efforts. The capabilities of the proposed approach are investigated through numerical examples concerning the solution accuracy and the computational effort.

Keywords: laminated plate, Carrera Unified Formulation, Legendre polynomials, node-dependent kinematics, finite element

1. Introduction

Composite laminated structures have attracted significant attention in the engineering field in the recent decades due to their outstanding structural efficiency. Due to the complex arrangement of these materials, conventional simulation tools soon reach their limits, which has boosted the demands for structural analysis methods to capture their mechanical responses accurately.

Towards the accurate analysis of thin-walled laminated structures, a variety of 2D theories

---

*Corresponding author. Tel: +39 0110906836, Fax: +39 0110906899.
Email address: `erasmo.carrera@polito.it` (E. Carrera)

have been proposed and extensively implemented in numerical models. Classical Plate Theory (CPT) [1] is the simplest 2D model, which is based on Kirchoff-Loves hypothesis. First-order Shear Deformation Theory (FSDT) [2] takes the transverse shear effects into account but can only approximate the shear stresses through the thickness of a plate as constants. A series of Higher-Order Theories (HOT) [3, 4, 5] have been suggested to improve the solution accuracy. Following this line, Carrera Unified Formulation [6] was introduced to derive refined plate and shell models for the analysis of laminated thin-walled structures. Various theories can be integrated to formulate refined kinematics based on either Equivalent Single Layer (ESL) or Layer-wise (LW) approach through the arbitrary sets of thickness functions. By making use of the so-called Fundamental Nucleus (FN), the corresponding governing equations can be derived in a unified and compact form [7]. In the CUF framework, a variety of 2D models constructed with different kinematic assumptions were introduced in the last years by Cinefra and Valvano [8], Cinefra et al. [9, 10, 11] and Carrera et al.[12].

In numerical analyses with finite elements (FE), a local refinement is often necessary to improve the numerical accuracy in the area with strong local effects such as stress concentration. Different approaches can be followed for this matter. A h-version approach [13, 14] increases the mesh refinement to capture local responses in detail, whereas a p-version refinement [15, 16, 17, 18] adopts shape functions with higher-order polynomials to approximate the structural deformation. The h-p-version approach uses these two methods in combination [19, 20, 21, 22]. Note that in these refinement methods, the kinematic assumption is invariant over the whole FE model.

The coupling of FE models with different kinematics has been discussed by many researchers. The three field formulations [23] enforce the displacement compatibility at domain interfaces with Lagrange multipliers. Various approaches have been developed based on this method, as presented by Aminpour et al. [24] who adopted a spline method, by Prager [25] who introduced an interface potential, as well as the eXtended Variational Formulation (XVF) suggested by Blanco et al. [26, 27, 28]. Application of a "multi-line" method was reported by Carrera and Pagani [29, 30]. A superimposed zone can also be used to bind the global and the local model. In Arlequin method, Lagrange multipliers are used to impose the compatibility in the overlapped area, as suggested by Dhia [31] and Dhia and Rateau [32]. Coupling of CUF-based 2D models with Arlequin method is reported by Biscani et al. [33, 34]. Differently, s-version refinement [35] superimposes additional elements on the global mesh, in which homogeneous boundary conditions were imposed on the borders of the overlapped zone. Based on the idea of overlapped

displacement field, the mathematical assumption can also be enriched locally in specific layers, as discussed in [36, 37, 38, 39].

Some techniques that can be used in global-local analyses are also provided in commercial software. Rigid Beam Element (RBE) and Multi-Point Constraints (MPCs) adopt linear functions to relate the displacements of the dependent and the independent nodes. A super-element can be built through grouping and condensing the degrees of freedom of a set of elements, and special treatment in the matrix operations is required. Shell-to-solid coupling employs a set of internally defined distribution coupling constraints to connect the edge nodes on a 2D model to those on a 3D model. Submodeling supports arbitrary mesh refinement, whereas it is a two-step in-series technique. Note that in the aforementioned global-local methods, usually two sets of FE mesh grids are needed to realize the local kinematic refinement.

The concept of Node-dependent Kinematics (NDK) was proposed for the local kinematic refinement of FE models, which can be used to formulate global-local models. The idea is that by relating the definition of thickness functions to the FE nodes, the kinematics can be refined locally on the chosen nodes. The nodal kinematics can be averaged and smeared over the in-plane domain of a 2D element naturally through the shape functions. Such an approach makes it possible to carry out the local kinematic refinement by merely increasing the kinematic order defined on the desired nodes without changing the mesh. Thus, one set of versatile FE mesh grids can be used to build a variety of global-local models without using any additional coupling approach. Carrera et al. [40] suggested NDK for refined 1D models first, then further applied to the modeling of laminated beams [41] and plates [42, 43, 44]. This technique was also used to model local structural features such as embedded piezoelectric skins and patches on composite plates [45] and beams [46]. In these works, it has been demonstrated that global-local models constructed with NDK can account for detailed local effects with fewer computational costs.

Szabó and Babuška [47] and Szabó et al. [18] introduced a series of hierarchical shape functions based on Legendre polynomials for the p-version elements. Such type of functions can trace back to [48, 49, 50]. The hierarchical functions for a quadrilateral domain were recently used for the refinement of cross-section kinematics on beam models by Pagani et al. [51] and Carrera et al. [52], and named as Hierarchical Legendre Expansions (HLE). To further exploit the numerical efficiency of HLE, in the present work, the authors introduce a novel class of 2D FE models for the global-local analysis of multilayered plates, which are based on a combination of NDK with a p-refinement scheme adopting higher-order Legendre polynomials. In the proposed method, the polynomial degree p will be treated as an input parameter of the FE model. In the following

3

sections, the theoretical basis is briefly explained, and the governing equations are derived from the Principle of Virtual Displacements (PVD). The efficiency of the proposed modeling approach is explored through several numerical cases on composite plates.
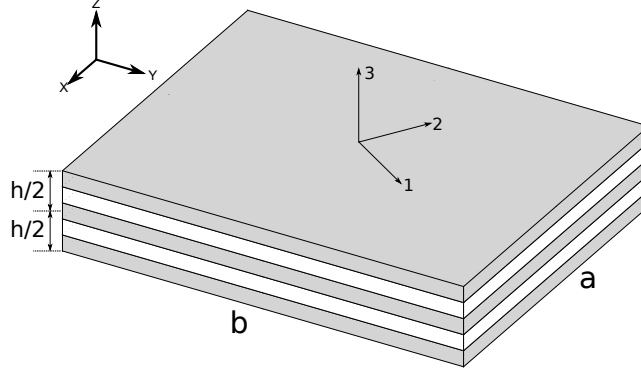
2. Preliminaries

Figure 1: Notation of a plate model for laminated structures.

The reference system and notation of a multilayered plate model are as shown in Figure 1. The strain and stress components can be arranged as:

$$\boldsymbol{\epsilon}_p^T = \{\epsilon_{xx}, \epsilon_{yy}, \epsilon_{xy}\}, \quad \boldsymbol{\epsilon}_n^T = \{\epsilon_{xz}, \epsilon_{yz}, \epsilon_{zz}\}. \tag{1}$$

$$\boldsymbol{\sigma}_p^T = \{\sigma_{xx}, \sigma_{yy}, \sigma_{xy}\}, \quad \boldsymbol{\sigma}_n^T = \{\sigma_{xz}, \sigma_{yz}, \sigma_{zz}\}. \tag{2}$$

where the subscript p and n indicate the in-plane and out-of-plane components, respectively. The strain vectors $\boldsymbol{\epsilon}_p$ and $\boldsymbol{\epsilon}_n$ can be obtained via the geometrical equations:

$$\boldsymbol{\epsilon}_p = \boldsymbol{D}_p \boldsymbol{u}, \qquad \boldsymbol{\epsilon}_n = (\boldsymbol{D}_{np} + \boldsymbol{D}_{nz})\boldsymbol{u}. \tag{3}$$

in which $\boldsymbol{D}_p$, $\boldsymbol{D}_{np}$ and $\boldsymbol{D}_{nz}$ are the differential operator matrices, and their explicit expressions are as follows:

$$\boldsymbol{D}_p = \begin{bmatrix} \partial_x & 0 & 0 \\ 0 & \partial_y & 0 \\ \partial_y & \partial_x & 0 \end{bmatrix}, \quad \boldsymbol{D}_{np} = \begin{bmatrix} 0 & 0 & \partial_x \\ 0 & 0 & \partial_y \\ 0 & 0 & 0 \end{bmatrix}, \quad \boldsymbol{D}_{nz} = \begin{bmatrix} \partial_z & 0 & 0 \\ 0 & \partial_z & 0 \\ 0 & 0 & \partial_z \end{bmatrix}. \tag{4}$$

4

The stress components can be attained through the constitutive equations as follows:

$$\boldsymbol{\sigma}_p = \tilde{\boldsymbol{C}}_{pp}\boldsymbol{\epsilon}_p + \tilde{\boldsymbol{C}}_{pn}\boldsymbol{\epsilon}_n, \qquad \boldsymbol{\sigma}_n = \tilde{\boldsymbol{C}}_{np}\boldsymbol{\epsilon}_p + \tilde{\boldsymbol{C}}_{nn}\boldsymbol{\epsilon}_n. \tag{5}$$

where $\tilde{\boldsymbol{C}}_{pp}$, $\tilde{\boldsymbol{C}}_{pn}$, $\tilde{\boldsymbol{C}}_{np}$, and $\tilde{\boldsymbol{C}}_{nn}$ are material coefficient matrices defined in the global system (x, y, z), and the original expressions of a single lamina in the material coordinate system $(1, 2, 3)$ read:

$$
\boldsymbol{C}_{pp} = \begin{bmatrix} C_{11} & C_{12} & C_{16} \\ C_{12} & C_{22} & C_{26} \\ C_{16} & C_{26} & C_{66} \end{bmatrix}, \qquad
\boldsymbol{C}_{pn} = \begin{bmatrix} 0 & 0 & C_{13} \\ 0 & 0 & C_{23} \\ 0 & 0 & C_{36} \end{bmatrix},
$$
$$
\boldsymbol{C}_{np} = \begin{bmatrix} 0 & 0 & 0 \\ 0 & 0 & 0 \\ C_{13} & C_{23} & C_{36} \end{bmatrix}, \qquad
\boldsymbol{C}_{nn} = \begin{bmatrix} C_{55} & C_{45} & 0 \\ C_{45} & C_{44} & 0 \\ 0 & 0 & C_{33} \end{bmatrix}.
\tag{6}
$$

The material coefficients are characterized by Young's moduli, the shear moduli, and the Poisson ratios.

3. Carrera Unified Formulation (CUF) for refined 2D models

In the framework of CUF, the displacement field of a plate structure can be assumed to be:

$$
\begin{aligned}
u(x, y, z) &= F_0(z)u_0(x, y) &&+ F_1(z)u_1(x, y) &&+ \cdots + F_N(z)u_N(x, y) \\
v(x, y, z) &= F_0(z)v_0(x, y) &&+ F_1(z)v_1(x, y) &&+ \cdots + F_N(z)v_N(x, y) \\
w(x, y, z) &= F_0(z)w_0(x, y) &&+ F_1(z)w_1(x, y) &&+ \cdots + F_N(z)w_N(x, y)
\end{aligned}
\tag{7}
$$

where the approximation functions $F_\tau(z)$ are also named as thickness functions. In a compact form, Equation 7 can be written as follows for ESL models:

$$\boldsymbol{u}(x, y, z) = F_\tau(z)\boldsymbol{u}_\tau(x, y) \qquad \tau = 0, 1, ..., N \tag{8}$$

in which $F_\tau(z)$ are defined on the domain through the whole thickness of the plate, which means $z \in [-\frac{h}{2}, \frac{h}{2}]$. Alternatively, for LW models, the displacements can be written as:

$$\boldsymbol{u}^k(x, y, \zeta_k) = F_\tau^k(\zeta_k)\boldsymbol{u}_\tau^k(x, y) \qquad \tau = 0, 1, ..., N \tag{9}$$

where k is the layer index, and $-1 \leq \zeta_k \leq 1$ is the adimensional thickness coordinate. The continuity conditions will be enforced at the layer interfaces.

One can observe that the number of expansion terms is $N + 1$ which is introduced as an input to the analysis. $\boldsymbol{u}_\tau^{(k)}(x, y)$ represent the unknown primary variables which are the factors corresponding to the expansion terms. The repeated indexes imply the application of Einstein's summation convention. Different from ESL models, in LW models the primary variables will be allocated to each layer. CUF provides a convenient and unified approach for the implementation of a variety of approximation theories to construct refined 2D kinematics for the analysis of multilayered structures, as described in Refs. [7, 8, 9].

3.1. ESL models based on Taylor expansions (TE)

In ESL models, Taylor series can be adopted as thickness functions by substituting $F_\tau = z^\tau (\tau = 0, 1, \cdots, N)$ into Equation 8, and the obtained thickness functions of the higher-order model read:

$$F_0 = z^0 = 1, \quad F_1 = z^1 = z, \quad \ldots, \quad F_N = z^N \tag{10}$$

Especially, FSDT [2] can be obtained as a particular case of the complete linear model ($N = 1$). Such type of theories based on Taylor expansions are the most commonly used in numerical analyses due to their inherent simplicity and low computational costs, and mostly they can be adequate to give solutions for global responses like gross displacements, natural frequencies, and buckling loads. The main limitation of TE when applied to the mechanical study of laminated structures is that, due to the intrinsic heterogeneity of multilayered structures, the obtained transverse shear stresses through the thickness might be discontinuous if no special treatment is applied.

3.2. LW models adopting Lagrange expansions (LE)

If F_τ^k are defined as Lagrange interpolation polynomials defined on layer k, as expressed in Equation 11, an LE-type LW model can be obtained. ζ_{k_τ} are located at the prescribed interpolation points. $\zeta_{k_0} = -1$ and $\zeta_{k_N} = 1$ in the natural reference system signifies the bottom and top surface of the kth layer, respectively.

$$F_\tau^k(\zeta_k) = \prod_{i=0, i \neq s}^{N} \frac{\zeta_k - \zeta_{k_i}}{\zeta_{k_\tau} - \zeta_{k_i}} \tag{11}$$

In LW models employing Lagrange expansions (LE), the displacements of each interpolation point are treated as unknown primary variables, and compatibility of the displacements at layer interfaces follows:

$$u_t^k = u_b^{k+1}, \qquad k = 1, \cdots, N_l - 1. \tag{12}$$

in which N_l is the total number of layers. The continuity of transverse stresses at layer interfaces can be achieved when a sufficient number of expansion terms are used in each layer, as demonstrated in the authors' previous work [9].
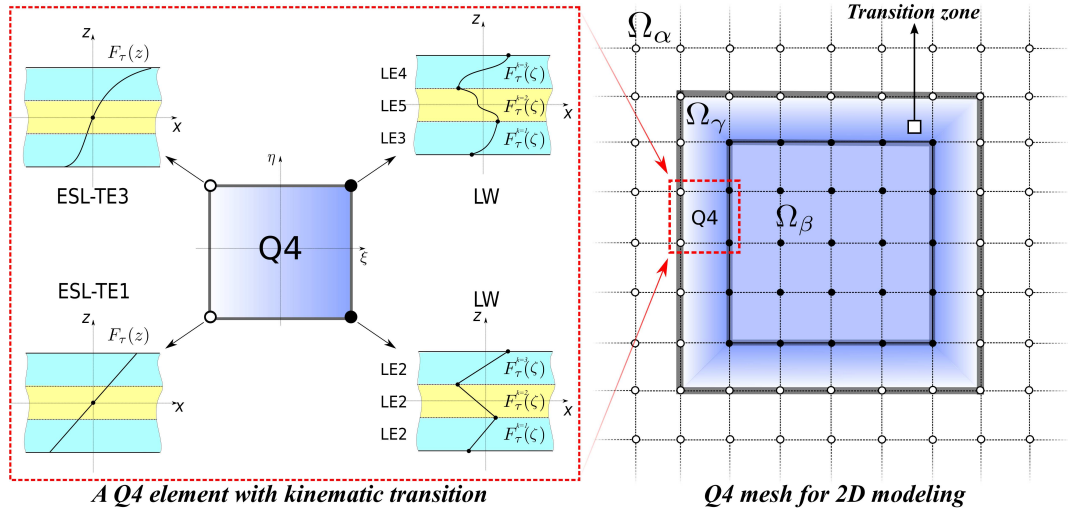
4. Plate elements Node-dependent Kinematics (NDK)

Figure 2: A Q4 plate element with node-dependent kinematics.

In CUF framework, the displacement functions of refined 2D FE models read:

$$\boldsymbol{u}^{(k)}(x,y,z) = N_i(x,y)F_\tau^{(k)}(z)\boldsymbol{u}_{i\tau} \qquad \tau = 0, \cdots, N; \quad i = 1, \cdots, M. \tag{13}$$

where $N_i(x,y)$ are the nodal shape functions, which for standard elements are Lagrange interpolation polynomials, and M is the total number of nodes per element. According to this definition, the nodal kinematics is defined uniformly over the whole FE model, which means a FE model with uniform kinematic assumptions. For structures undergoing high-stress gradients only within a limited region, such models might consume some unnecessary computational resources.

7

Carrera et al. [40, 41] proposed a method to define the local kinematic refinement in FE models. By relating the thickness functions to the chosen nodes through Equation 14, an element consisting of more than one type of mathematical assumptions can be formulated:

$$\boldsymbol{u}^{(k)}(x,y,z) = N_i(x,y)F_\tau^{i(k)}(z)\boldsymbol{u}_{i\tau} \qquad \tau = 0,\cdots,N; \quad i = 1,\cdots,M. \tag{14}$$

in which $F_\tau^{i(k)}$ are defined on node i and become kinematics local to the node. The kinematics of a certain node i is indeed smeared over the finite element domain utilizing the shape functions $N_i(x,y)$. In a sense, node i acts as the "anchor" of $F_\tau^{i(k)}$ within the 2D mesh. A natural application of this approach is to construct global-local FE models. Assume that the kinematics is gradually refined from one side to the other side of an element, as illustrated on the left-hand side of Figure 2, an element with a kinematic transition can be formulated. The transition zone Ω_γ can serve as a bridge between the local domain Ω_β with refined kinematics and a peripheral domain Ω_α with lower-order kinematics, as illustrated on the right-hand side of Figure 2. In such a way, the local kinematic refinement can be carried out straightforwardly without changing the mesh nor using any extra coupling approach. Thus, the compactness of the governing equation is kept, and the implementation of simultaneous multi-model global-local FE models is very convenient. On the other hand, this approach enables a set of mesh grids to accommodate a series of local refinement schemes, from very simple and cheap to very precise but computationally expensive. Moreover, the convenience of changing the nodal mathematical assumptions permits an automatic refinement procedure without user intervention. NDK has been successfully applied to generate numerically efficient global-local models for 1D [40, 41] and 2D [42, 43, 44, 45] modeling in the analysis of multilayered structures.

5. Higher-order Legendre polynomials as the shape functions of plate elements

Szabó et al. [18] suggested a set of shape functions based on Legendre polynomials for a quadrilateral domain $(\xi, \eta) \in [-1, 1]$. This type of shape functions consist of *nodal modes*, *edge modes*, and *internal modes*, as shown in Figure 3.

Nodal modes are defined as Lagrange linear interpolation polynomials on the four vertex nodes of the quadrilateral domain, and their expressions are:

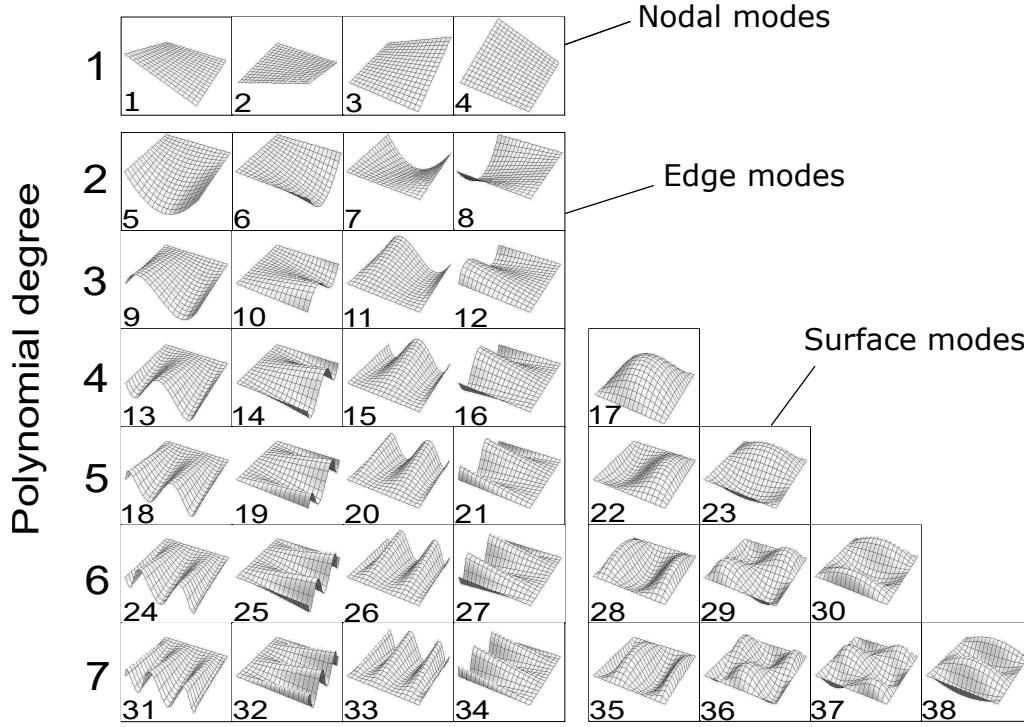$$N_i(\xi,\eta) = \frac{1}{4}(1 - \xi_i\xi)(1 - \eta_i\eta) \qquad i = 1, 2, 3, 4 \tag{15}$$

8

Figure 3: High order Legendre polynomials as shape functions of plate elements.

where (ξ_i, η_i) represent the local coordinates of node i in the isoparametric reference system in a four-node element.

Edge modes are dominated by the deformation on the four edges and vanish linearly along the corresponding perpendicular edges. These functions are expressed as:

$$
\begin{aligned}
N_i(\xi, \eta) &= \frac{1}{2}(1 - \eta)\phi_p(\xi) && i = 5, 9, 13, 18, \cdots \\
N_i(\xi, \eta) &= \frac{1}{2}(1 + \xi)\phi_p(\eta) && i = 6, 10, 14, 19, \cdots \\
N_i(\xi, \eta) &= \frac{1}{2}(1 + \eta)\phi_p(\xi) && i = 7, 11, 15, 20, \cdots \\
N_i(\xi, \eta) &= \frac{1}{2}(1 - \xi)\phi_p(\eta) && i = 8, 14, 16, 21, \cdots
\end{aligned}
\tag{16}
$$

where ϕ_p is defined as:

$$
\phi_p(\xi) = \sqrt{\frac{2p-1}{2}} \int_{-1}^{\xi} L_{p-1}(x)dx = \frac{L_p(\xi) - L_{p-2}(\xi)}{\sqrt{4p-2}} \quad p = 2, 3, \cdots
\tag{17}
$$

Surface modes contain the deformation shapes that happen on the internal surface and

9

vanish on the edges:

$$N_i(\xi, \eta) = \phi_m(\xi)\phi_n(\eta) \qquad m, n \geqslant 2; \quad i = 17, 22, 23, 28, 29, 30, \cdots \tag{18}$$

With the above-described hierarchical shape functions, four-node Legendre-type elements for p-refinement can be developed. Different from Lagrange-type shape functions, when the polynomial degree p increases to $p+1$, only the newly added shape functions and the resulting matrices need to be introduced. Meanwhile, it should be noticed that compared with Lagrange polynomials of the same polynomial order interpolated on equally spaced internal nodes, Legendre-type shape functions usually requires a fewer number of functions in the construction of a 2D element. Furthermore, for Legendre-type shape functions the polynomial order p is defined as an input parameter and p-refinement can be conveniently realized on the same set of mesh grids to reach the numerical convergence.

6. FE governing equations

In this section, the governing equations for plate elements with NDK are derived from the Principle of Virtual Displacements (PVD). For a static problem, one has:

$$\delta L_{int} = \delta L_{ext} \tag{19}$$

where δL_{int} is the strain energy due to the external load, and δL_{ext} represents the work done by the external load on the virtual displacements. The internal work can be expressed as:

$$\delta L_{int} = \int_V \delta\boldsymbol{\epsilon}^T \boldsymbol{\sigma} dV = \int_\Omega \int_{A_k} \delta\boldsymbol{\epsilon}^T \boldsymbol{\sigma} dA_k d\Omega \tag{20}$$

in which Ω represents the element in-plane domain, and A_k indicates the thickness domain within layer k. In Equation 20, the integration is conducted within the domain determined by the element and the layer k. The displacement field can be expressed as shown in Equation 21 for ESL models, in which $z \in [z_{bottom}, z_{top}]$:

$$\begin{aligned}
\boldsymbol{u}(x, y, z) &= N_i(x, y)F_\tau^i(z)\boldsymbol{u}_{i\tau} \qquad \tau = 1, \cdots, N; \quad i = 1, \cdots, M. \\
\delta\boldsymbol{u}(x, y, z) &= N_j(x, y)F_s^j(z)\delta\boldsymbol{u}_{js} \qquad s = 1, \cdots, N; \quad j = 1, \cdots, M.
\end{aligned} \tag{21}$$

10

Alternatively, for LW models as in Equation 22 , where $\zeta_k \in [-1, 1]$:

$$\boldsymbol{u}^k(x, y, \zeta_k) = N_i(x, y)F_\tau^{ik}(\zeta_k)\boldsymbol{u}_{i\tau}^k \qquad \tau = 1, \cdots, N; \quad i = 1, \cdots, M.$$
$$\delta\boldsymbol{u}^k(x, y, \zeta_k) = N_j(x, y)F_s^{jk}(\zeta_k)\delta\boldsymbol{u}_{js}^k \qquad s = 1, \cdots, N; \quad j = 1, \cdots, M. \tag{22}$$

The strain vectors can be obtained through Equation 23, which applies to both ESL and LW models:

$$\boldsymbol{\epsilon}_p^k = F_\tau^{i(k)}\boldsymbol{D}_p N_i \boldsymbol{u}_{i\tau}^{(k)}$$
$$\boldsymbol{\epsilon}_n^k = F_\tau^{i(k)}\boldsymbol{D}_{np} N_i \boldsymbol{u}_{i\tau}^{(k)} + F_{\tau,z}^{i(k)} N_i \boldsymbol{u}_{i\tau}^{(k)} \tag{23}$$

Considering the strains as expressed in Equation 23 and the constitutive relations in Equation 5, one can obtain the expression of the internal work as:

$$\delta L_{int} = \int_\Omega \int_{A_k} (\delta\boldsymbol{\epsilon}_n^{k^T}\boldsymbol{\sigma}_n^k + \delta\boldsymbol{\epsilon}_p^{k^T}\boldsymbol{\sigma}_p^k)dA_k d\Omega = \delta\boldsymbol{u}_{js}^{(k)^T}\boldsymbol{K}_{ij\tau s}^k\boldsymbol{u}_{i\tau}^{(k)} \tag{24}$$

in which the 3×3 matrix $\boldsymbol{K}_{ij\tau s}^k$ is the so-called *fundamental nucleus* (FN) of stiffness in the context of CUF, which is the basic unit of the element stiffness matrix. Thus, the stiffness matrix of the spatial domain identified by Ω and A_k can be obtained.

Assume that $p_\alpha(x, y)$ is a surface load acting on a horizontal surface of the plate (α indicates the loading direction, which is x, y or z), the virtual variation of the external work caused by p_α can be written as:

$$\delta L_{ext}^{p_\alpha} = \int_\Omega \delta u_\alpha^{(k)} p_\alpha d\Omega = \int_\Omega \delta u_{\alpha_{js}}^{(k)} N_j F_s^{j(k)}(z_p) p_\alpha d\Omega \tag{25}$$

where z_p represents the coordinate of the loading surface. If the external surface load is written into a vector $\boldsymbol{p}_\alpha(x, y)$, Equation 25 can be further written as Equation 26, where $\boldsymbol{P}_{js}^{(k)}$ is the FN of external load. In $\boldsymbol{P}_{js}^{(k)}$, only the components on α direction are non-zero.

$$\delta L_{ext}^{p_\alpha} = \delta\boldsymbol{u}_{js}^{(k)^T}\boldsymbol{P}_{js}^{(k)} \tag{26}$$

Hence, the governing equation can be obtained as:

$$\delta\boldsymbol{u}_{js}^{(k)^T} : \quad \boldsymbol{K}_{ij\tau s}^k\boldsymbol{u}_{i\tau}^{(k)} = \boldsymbol{P}_{js}^{(k)} \tag{27}$$

If the external loads are point loads, $\boldsymbol{P}_{js}^{(k)}$ can be expressed accordingly then be substituted

11

into Equation 27. For the explicit expressions of the FNs, the reader is referred to [42].

7. Assembly of the stiffness matrix and load vector

The fundamental nucleus (FN) is a core unit of the stiffness matrix. By looping on the indexes of the expansions, the stiffness matrices on the node level can be obtained, then be further assembled on the element level and the global structure. For more details on the assembly technique of CUF-based FE models, see Carrera et al. [7].

In fact, it is quite straightforward to apply such a routine to the NDK cases. When various nodal kinematic assumptions coexist in an element, sub-matrix K_{ij} will probably be rectangular rather than square. As an example, Figure 4 illustrates the assembly of the stiffness sub-matrices and load vector in a NDK-type Q4 plate element el. In this element, on node a and d LW models are employed, while on node b and c ESL models are adopted. Consider two typical cases of the sub-matrices:

- $\boldsymbol{K}_{aa}$: diagonal matrix for LW models on node a, which has a different number of expansions from Layer 1 to Layer 3. $\boldsymbol{K}_{aa}$ is achieved by assembling the stiffness matrices corresponding to each layer then superimposing the interfacial components.

- $\boldsymbol{K}_{bb}$: diagonal matrix for ESL models for node b, obtained by overlapping the stiffness matrices of all the layers directly.

- $\boldsymbol{K}_{ab}$ and $\boldsymbol{K}_{ba}$: coupling matrices between node a and b. Since when PVD is applied the integration to obtain the stiffness matrix is operated on a brick domain defined by element el and layer k, $\boldsymbol{K}_{ab}^k$ and $\boldsymbol{K}_{ba}^k$ (k is the layer index) will become rectangular. After the components at layer interfaces are overlapped, the location of their components become as shown in Figure 4, where $\boldsymbol{K}_{ab}^1$, $\boldsymbol{K}_{ab}^2$, and $\boldsymbol{K}_{ab}^3$ are in a banded shape.

Meanwhile, the load vector will be assembled similarly, and become compatible with the stiffness matrix, as shown on the right-hand-side of Figure 4.

8. Numerical results

In this section, results on laminated structures obtained from p-version elements constructed with higher-order Legendre polynomials and NDK are reported. Firstly, in Case 1, composite laminates under sinusoidal distributed pressure are analyzed, and the Legendre-type elements using CUF-based kinematics are validated on both thick and thin plates. Case 2 presents laminated
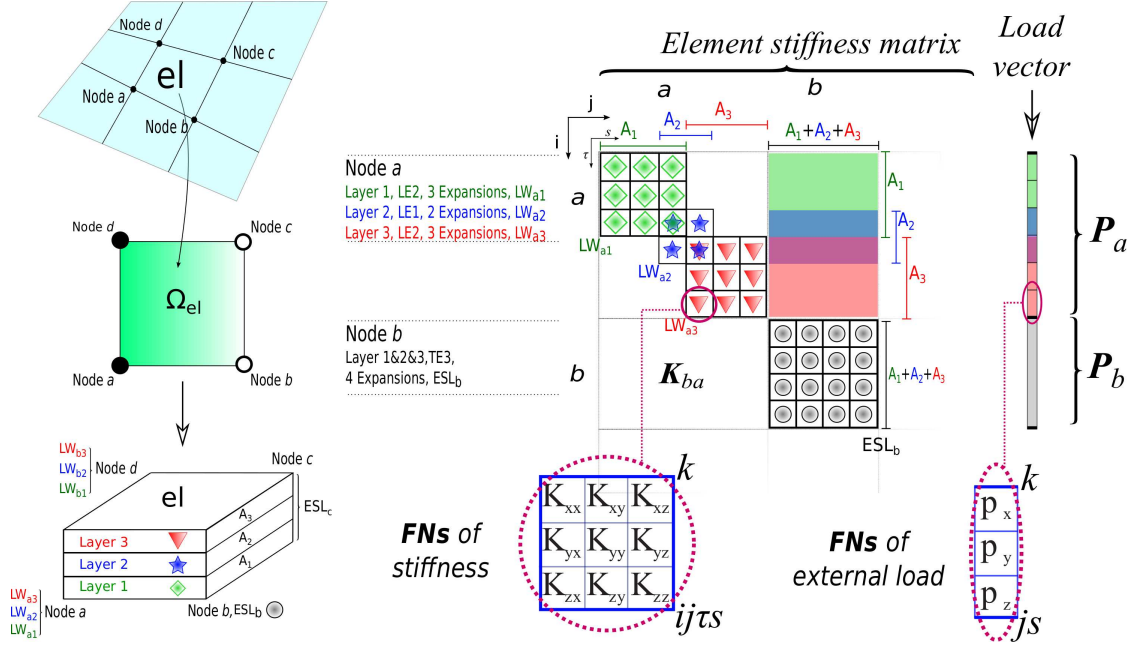
12

Figure 4: Assembly of the stiffness matrix and load vector of elements with various nodal kinematics.

plates under an out-of-plane point load, which causes intense local deformation. In Case 3, a simply supported plate under local pressure is studied, and NDK is used to build a computationally efficient FE model.

In the authors' previous work [51, 52], the same set of higher-order Legendre polynomials have been denoted as "HLE" when used as cross-section functions of refined beam models. Following this notation, in the present article, FE models employing Legendre-type shape functions of the pth order will be represented by HLEp. Meanwhile, TEn is used to indicate TE-type kinematics of the nth order, and LEn serves LE-type thickness functions with Lagrange polynomials of order n. For FE models with multiple kinematics, LEm/TEn is used as an acronym.

8.1. Case 1: Simply-supported three-layered cross-ply plates under pressure load

By referring to Pagano's work [53], three-layered composite plates with lamination sequence $[0°/90°/0°]$ under bi-sinusoidal transverse pressure and simple supports are studied. The load is imposed on the top surface, whose distribution follows:

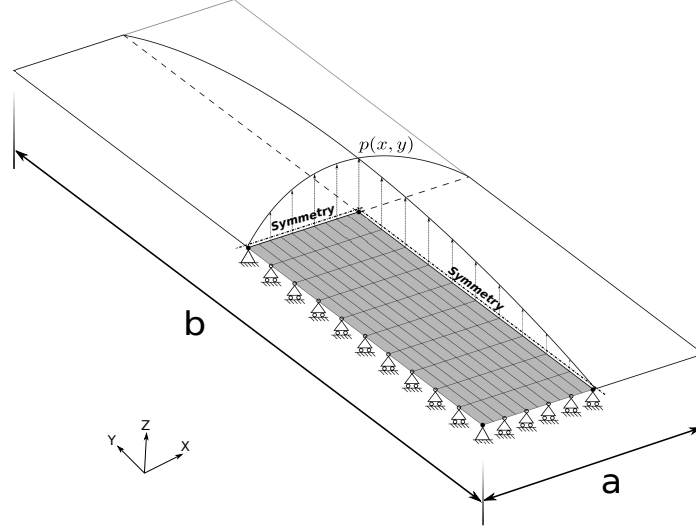$$p(x, y) = p_0 \cdot \sin(\frac{\pi x}{a}) \sin(\frac{\pi y}{b}) \tag{28}$$

13

Figure 5: 2D FE model for the composite plate, with symmetry boundary conditions.

The plates are rectangular with $b = 3a$. The nondimensional material coefficients used for each layer are: $E_L = 25$, $E_T = 1$, $G_{LT} = 0.5$, $G_{TT} = 0.2$, $\nu_{LT} = \nu_{TT} = 0.25$, where L and T stand for the fiber longitudinal and transverse direction, respectively. The three layers have equal thickness $h/3$. Both thick ($a/h = 2$) and thin ($a/h = 100$) plates are considered. For the convenience of comparison, the displacement and stresses are non-dimensionalized according to:

$$
\begin{aligned}
\bar{w} &= \frac{100 E_T h^3}{p_0 a^4} w, \qquad \bar{\sigma}_{xx} = \frac{h^2}{p_0 a^2} \sigma_{xx}, \qquad \bar{\sigma}_{yy} = \frac{10 h^2}{p_0 a^2} \sigma_{yy}, \qquad \bar{\sigma}_{xy} = \frac{10 h^2}{p_0 a^2} \sigma_{xy}, \\
\bar{\sigma}_{xz} &= \frac{10 h}{p_0 a} \sigma_{xz}, \qquad \bar{\sigma}_{yz} = \frac{10 h}{p_0 a} \sigma_{yz}, \qquad \bar{\sigma}_{zz} = \frac{1}{p_0} \sigma_{zz}.
\end{aligned}
\tag{29}
$$

The following constraints are used on the edges to satisfy the boundary conditions:

$$
\begin{aligned}
At \quad x &= 0, a : \qquad v = w = 0; \\
At \quad y &= 0, b : \qquad u = w = 0.
\end{aligned}
\tag{30}
$$

Taking advantage of the symmetry feature of the structure and loading conditions, a quarter of the plate is modeled with finite elements with the help of symmetric boundary conditions, as illustrated in Figure 5. Numerical study on such a case has also been reported by many authors. Carrera et al. [9] studied this case with MITC9 finite elements employing various CUF-based models; Kulikov and Plotnikova [54] also proposed solutions obtained with the so-called Sampling-surfaces method (SaS). Their solutions are also listed in Table 1 and Table 2 for comparison in which the displacement and stress evaluations are summarized.

14

The results obtained with the proposed p-version elements adopting higher-order Legendre polynomials are compared against those achieved with nine-node Lagrange-type elements (Q9) with full integration. Lagrange polynomials of the $4th$ order (LE4) are used as thickness functions in each layer. To achieve numerical convergence, for FE models based on Q9 elements, the mesh is refined gradually, following a h-refinement scheme. For Legendre-type elements, the polynomial order p of the elements is increased hierarchically.

The thick plate ($a/h = 2$) is first studied. From Table 1, it can be found that FE model with 5×5 Q9 elements or one HLE7 element can lead to converged numerical results. It should be noticed that, comparatively, an HLE7 element uses a fewer number of degrees of freedom than 5×5 Q9 elements. Regarding the relative error of $\bar{\sigma}_{yz}$ with respect to the degrees of freedom, as shown in Figure 6 (a), it is evident that FE models adopting Legendre-type elements have better numerical efficiency than commonly used Lagrange-type Q9 elements.

Table 1: Displacement and stress evaluation on the three-layered cross-ply plates under pressure load, obtained with LE4 as thickness functions, thick plate case ($a/h = 2$).

Element	Mesh	$\bar{w}$ $\left(\frac{a}{2}, \frac{b}{2}, 0\right)$	$\bar{\sigma}_{yy}$ $\left(\frac{a}{2}, \frac{b}{2}, \frac{h}{6}\right)$	$10\bar{\sigma}_{yz}$ $\left(\frac{a}{2}, 0, 0\right)$	$\bar{\sigma}_{zz}$ $\left(\frac{a}{2}, \frac{b}{2}, \frac{h}{2}\right)$	DOFs
Q9	1×1	3.196	1.006	2.668	0.5103	351
Q9	2×2	8.167	2.356	7.525	1.010	975
Q9	4×4	7.882	2.315	6.904	0.9693	3159
Q9	5×5	8.165	2.308	6.825	1.004	4719
HLE2	1×1	8.137	2.671	9.853	1.038	312
HLE3	1×1	8.005	2.866	6.961	0.9598	468
HLE4	1×1	8.120	2.333	6.600	0.9918	663
HLE5	1×1	8.167	2.279	6.622	1.004	897
HLE6	1×1	8.166	2.293	6.688	1.004	1170
HLE7	1×1	8.165	2.295	6.686	1.004	1482
Pagano [53]		8.17	2.30	6.68	–	
Kulikov and Plotnikova [54]		8.1659	2.6772	6.6778	1.0001	
Carrera et al. [9]		8.166	2.296	6.690	1.000	

For the thin plate case ($a/h = 100$), the Q9 elements with full integration encountered some locking, which can be observed from the transverse shear stress $\bar{\sigma}_{yz}$ shown in both Table 2 and Figure 6(b). For Legendre-type elements, with the increase of the polynomial order p, the accuracy can also be improved gradually. Table 2 shows that with even only one element (mesh 1×1), HLE8 can give very accurate stress evaluation. If a h-p-refinement scheme (mesh 2×2) is used, the accuracy of the stress solutions is further enhanced. Moreover, the use of higher-order functions mitigates the locking issues, which shows that in this case, HLE8 can

15

deform appropriately to capture the responses of the thin plate. Concerning the variation of the transverse shear stress $\bar{\sigma}_{yz}$ as shown in Figure 6 (b), one can observe that Legendre-type elements still convergence faster than the Q9 elements for the thin plate case.
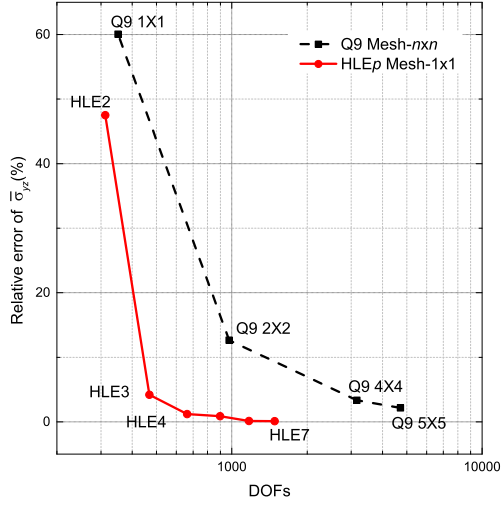
Table 2: Displacement and stress evaluation on the three-layered cross-ply plates under pressure load, obtained with LE4 as thickness functions, thin plate case ($a/h = 100$).

| Element	Mesh	$\bar{w}$ $(\frac{a}{2}, \frac{b}{2}, 0)$	$\bar{\sigma}_{yy}$ $(\frac{a}{2}, \frac{b}{2}, \frac{h}{6})$	$10\bar{\sigma}_{yz}$ $(\frac{a}{2}, 0, 0)$	$\bar{\sigma}_{zz}$ $(\frac{a}{2}, \frac{b}{2}, \frac{h}{2})$	DOFs
Q9	5×5	0.5069	0.2511	2.365	1.813	4719
Q9	10×10	0.5076	0.2528	2.217	1.128	17199
Q9	15×15	0.5076	0.2530	2.020	1.041	37479
HLE3	1×1	0.4487	0.5085	105.1	5.404	468
HLE4	1×1	0.5054	0.3479	42.23	-1.431	663
HLE5	1×1	0.5087	0.2830	-7.019	0.4908	897
HLE6	1×1	0.5077	0.2486	0.8042	1.164	1170
HLE7	1×1	0.5077	0.2531	1.202	1.011	1482
HLE8	1×1	0.5077	0.2532	1.087	0.9971	1833
HLE3	2×2	0.5075	0.3472	8.386	2.541	1287
HLE4	2×2	0.5075	0.2629	3.799	0.8828	1911
HLE5	2×2	0.5077	0.2540	0.9318	0.9758	2691
HLE6	2×2	0.5077	0.2530	1.075	1.003	3627
HLE7	2×2	0.5077	0.2531	1.084	1.000	4719
HLE8	2×2	0.5077	0.2531	1.084	1.000	5967
Pagano [53]		0.508	0.253	1.08	–	
Kulikov and Plotnikova [54]		0.50766	0.25236	1.0836	1.000	
Carrera et al. [9]		0.5077	0.2533	1.085	1.000	

The best solutions to the transverse shear stresses obtained with h-refinement using Q9 and p-refinement are compared in Figure 7 regarding the variation in the thickness direction, and they are in high agreement with each other. The contour plots of σ_{xz} shown in Figure 8 demonstrate that even with only one element, when the polynomial degree p is sufficiently high, Legendre-type elements adopting CUF-based kinematics can capture very detailed 3D stress field with satisfying accuracy for both of the thick and thin plate cases.

8.2. Case 2: Simply supported three-layered plates subjected to a point load

Three-layered square cross-ply plates under simple supports on the four edges are considered in this part. The plates are subjected to a concentrated load at the central point on the top surface, as illustrated in Figure 9. The three layers are of equal thickness $h/3$ and laminated in the sequence [0°/90°/0°]. The mechanical properties of each lamina are characterized by
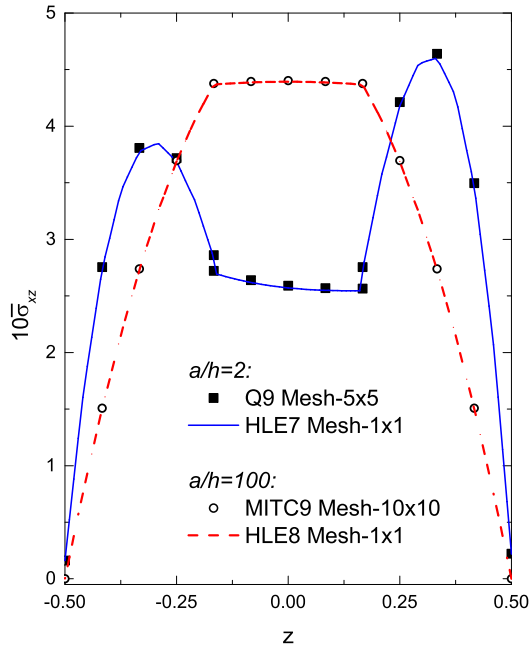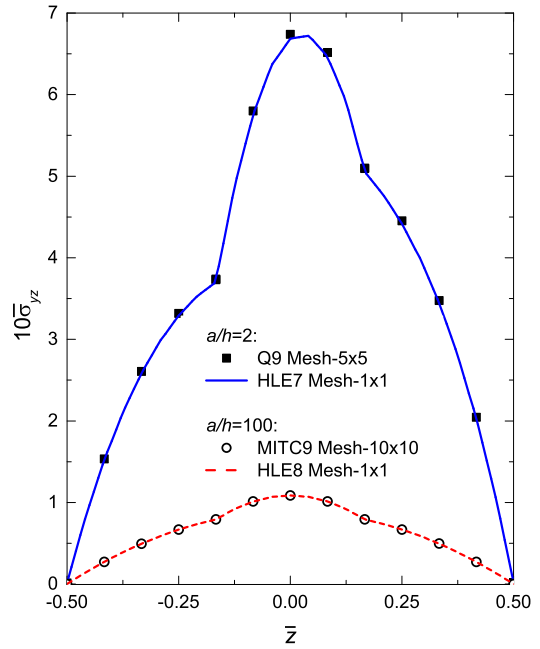
(a) Thick plate, $a/h = 2$
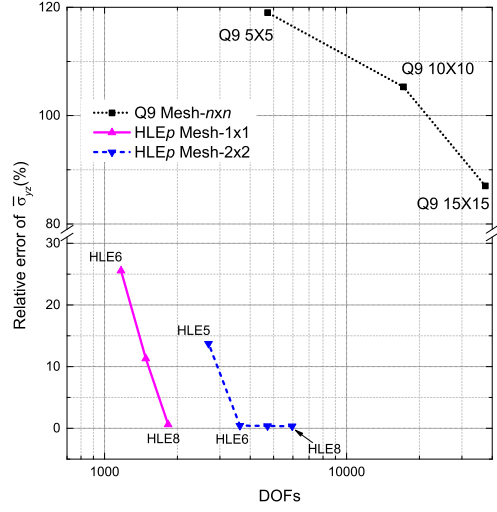
(b) Thin plate, $a/h = 100$

Figure 6: Relative error of $\bar{\sigma}_{yz}$ on the three-layered cross-ply plates under pressure load, obtained with LE4 as thickness functions.

(a) $\bar{\sigma}_{xz}$ at $(0, \frac{b}{2}, \bar{z})$

(b) $\bar{\sigma}_{yz}$ at $(\frac{a}{2}, 0, \bar{z})$

Figure 7: Through-the-thickness variation of the transverse shear stresses on the plates under sinusoidal pressure.
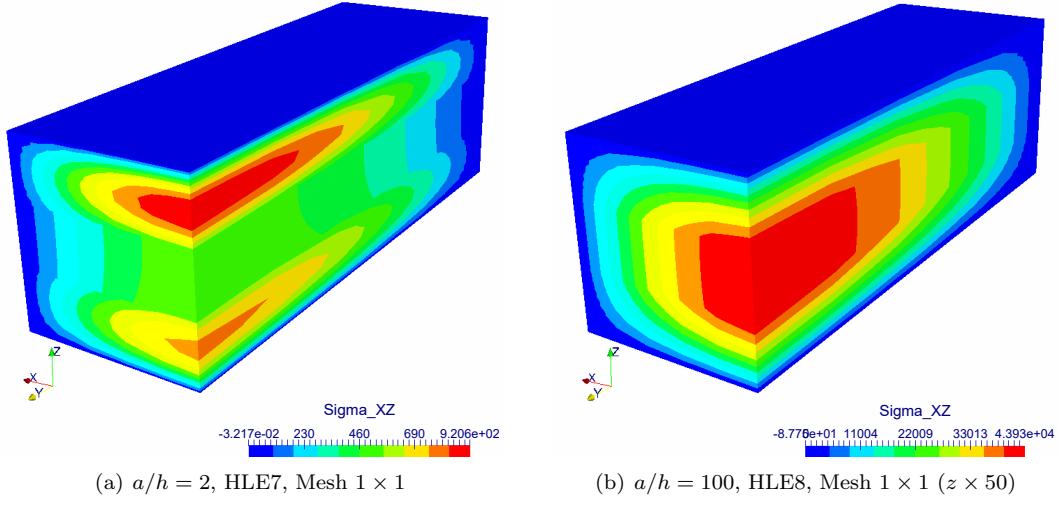
17

(a) $a/h = 2$, HLE7, Mesh 1×1 (b) $a/h = 100$, HLE8, Mesh 1×1 ($z \times 50$)

Figure 8: Contour plot of σ_{xz} obtained with Legendre-type elements employing LE4 as thickness functions.

nondimensional coefficients: $E_L = 25$, $E_T = 1$, $G_{LT} = 0.5$, $G_{TT} = 0.2$, $\nu_{LT} = \nu_{TT} = 0.25$, where L denotes the fiber direction and T its transverse direction. Both thick ($a/h = 4$) and thin ($a/h = 100$) cases are studied. The simple supports are defined following Equation 30. The closed-form reference solutions are provided by Carrera and Ciuffreda [55]. The transverse displacements w are reported, which are non-dimensionalized as:

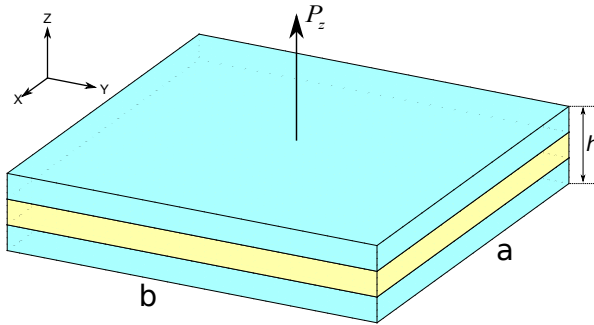$$\bar{w} = \frac{100 E_T h^3}{P_z a^2} w \tag{31}$$

Figure 9: Geometry and loading of the simply-supported laminated plates subjected to a point load.

Point loads cause high local deformations, which represent a severe challenge for structural

18

analyses based on weak-form solution techniques. Through this numerical example, the capabilities of Legendre-type elements in approximating the concentration effects are investigated. In the FE model, the plates are discretized into 16 (4×4) Legendre-type plate elements, as shown in Figure 10. The plates are firstly analyzed with Legendre-type elements adopting CUF-based thickness kinematics LE4 in each layer, and the polynomial order in each element is increased gradually until 8. Then, by applying NDK, LE4 kinematics is restricted in the area surrounding the loaded point, leaving the remaining part the of the structure with kinematics based on TEn. The corresponding assignment of nodal kinematics is illustrated in Figure 10.
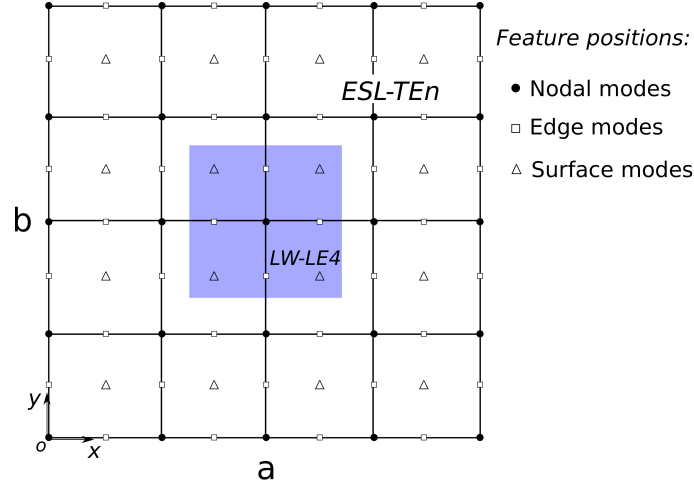

Figure 10: Assignment of nodal kinematics on the FE model for the three-layered plates subjected to a point load.

The variation of the vertical displacement $\bar{w}$ through the thickness of the plates is shown in Figure 11. It can be observed that, when LE4 kinematics is adopted uniformly on the whole FE model, the quality of the solutions improves with the increase of the polynomial order of the elements. For the thick plate case with $a/h = 4$, when elements of a higher-order are used, the displacement at the loading point shoots up, which demonstrates that the strong local deformation can be better captured with higher-orders in p-version refinement. Comparatively, for the thin plate case with $a/h = 100$, the local effects through the thickness at the loading point are much less significant.

Since the local effects take place within only a limited area near the loading point, for the peripheral region less-refined kinematics is sufficient. The results obtained with global-local models constructed with NDK are reported in Figure 11 and Table 3. The results show that the higher-order elements can accommodate severe deformations when employing refined kinematics.

19

In the meanwhile, the NDK models can lead to comparable accuracy with the most refined uniform kinematic models while reducing the computational costs concerning the degrees of freedom.
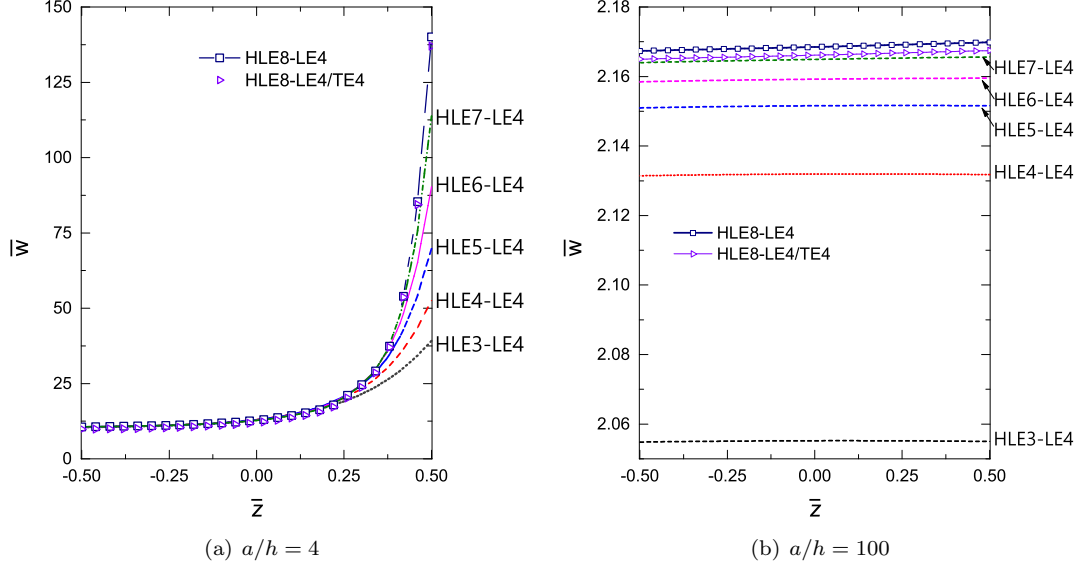

(a) $a/h = 4$ (b) $a/h = 100$

Figure 11: Through-the-thickness variation of $\bar{w}$ at $(a/2, b/2)$ on the three-layered plates subjected to a point load.

Table 3: $\bar{w}$ at $(\frac{a}{2}, \frac{b}{2}, 0)$ on the simply-supported laminated plates subjected to a point load.

Element	Kinematics	$\bar{w}(a/h = 4)$	$\bar{w}(a/h = 100)$	DOFs
HLE8	LE4	12.80	2.169	21255
HLE8	LE4/FSDT	10.96	2.167	5751
HLE8	LE4/TE2	11.04	2.165	7575
HLE8	LE4/TE3	11.88	2.166	8943
HLE8	LE4/TE4	11.95	2.166	10311
Carrera and Ciuffreda [55]		13.188	2.172	–

8.3. Case 3: Three-layered cross-ply moderate thick composite plate under local pressure

This case includes a square cross-ply plate imposed to a local pressure load in the central area of its top surface, as shown in Figure 12. The length of the edges are $a = b = 0.1m$ and the edge-to-thickness ratio is $a/h = 10$. The stacking sequence is $[0°/90°/0°]$ and each layer has equal thickness. The uniformly distributed pressure load p_0 covers the area of $a/5 \times b/5$. The plate is simply supported on its four edges, and the corresponding constraints are set with reference

20

to Equation 30. The mechanical properties of the material for each layer are: $E_L = 132.5$GPa, $E_T = 10.8$GPa, $\nu_{LT} = 0.24$, $\nu_{TT} = 0.49$, $G_{LT} = 5.7$GPa, and $G_{TT} = 3.4$GPa.
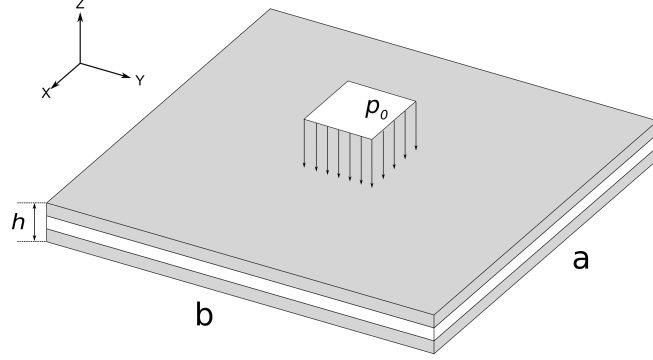

Figure 12: Geometry and loading of the three-layered cross-ply composite plate under local pressure, with $a/h = 10$ and $[0°/90°/0°]$.

Exploiting the symmetries of the problem, a FE model of a quarter of the structure is built, which consists of 5×5 Legendre-type elements, as shown in Figure 13. The displacement and stresses are evaluated on four points, whose locations are indicated in Figure 13 and explicitly given in Table 4. Firstly, different polynomial orders p are tested using LE4 as thickness functions. Then, the computational efforts are reduced by making use of an NDK methodology. In the area distant from the loading region, less-refined model FSDT is employed, leading to a global-local model as shown in Figure 13.

The numerical results are summarized in Table 4. The reference solutions proposed by Biscani et al. [33] and Zappino et al. [43] are also listed for comparison. From the results in Table 4, it can be found that the numerical convergence is achieved when the polynomial order p reaches 6. The global-local model also gives accurate estimation in the loaded region. The through-the-thickness variation of the transverse shear stresses obtained with a LE4 model and NDK model LE4/FSDT are plotted in Figure 14. It can be observed that in the loaded local zone, the model with LE4/FSDT can lead to results in high agreement with the model adopting uniform LE4 kinematics, but with much fewer degrees of freedom.

9. Conclusions

In this work, plate elements adopting higher-order Legendre polynomials as shape functions are explored and used in combination with Node-dependent Kinematics (NDK) for the analysis of multilayered structures. The following conclusions can be drawn based on the numerical study:
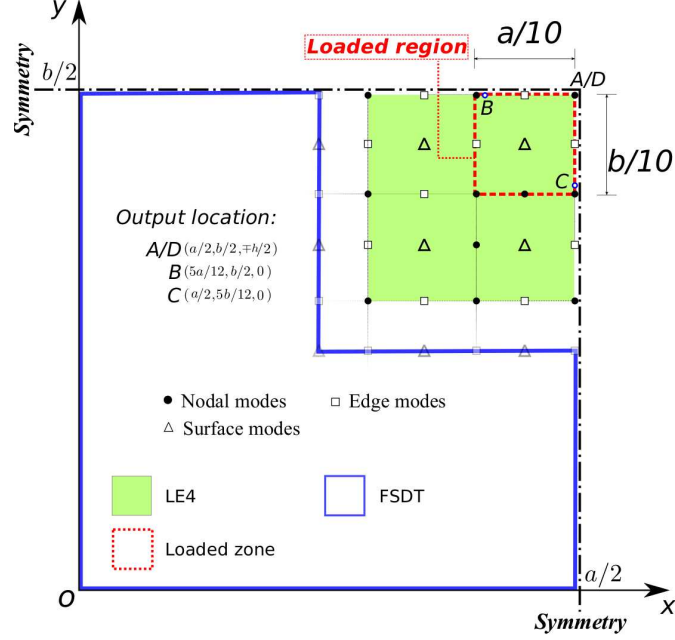
Figure 13: Assignement of nodal kinematics on the FE model for the three-layered cross-ply composite plate under local pressure.

Table 4: Displacement and stress evaluation on the three-layered plate under local pressure.

Element	Mesh	Kinematics	$w[10^{-5}\text{m}]$ $A(\frac{a}{2}, \frac{b}{2}, \frac{-h}{2})$	$\sigma_{xx}[\text{MPa}]$ $A(\frac{a}{2}, \frac{b}{2}, \frac{-h}{2})$	$\sigma_{yy}[\text{MPa}]$ $A(\frac{a}{2}, \frac{b}{2}, \frac{-h}{2})$	$-10\sigma_{xz}[\text{MPa}]$ $B(\frac{5a}{12}, \frac{b}{2}, 0)$	$-10\sigma_{yz}[\text{MPa}]$ $C(\frac{a}{2}, \frac{5b}{12}, 0)$	$-\sigma_{zz}[\text{MPa}]$ $D(\frac{a}{2}, \frac{b}{2}, \frac{h}{2})$	DOFs
HLE3	5×5	LE4	1.681	12.08	2.061	6.596	7.094	1.241	6084
HLE4	5×5	LE4	1.682	11.92	2.023	6.501	6.965	0.881	9399
HLE5	5×5	LE4	1.682	11.97	2.039	6.497	6.972	1.045	13689
HLE6	5×5	LE4	1.682	11.98	2.037	6.499	6.974	1.003	18954
HLE6	5×5	FSDT	1.610	10.44	1.850	3.829	4.647	0.938	2430
HLE6	5×5	LE4/FSDT	1.702	12.50	2.036	6.516	6.941	1.008	5592
Biscani et al. [33]			1.674	11.94	2.019	6.524	−	−	−
Zappino et al. [43]			1.675	11.99	2.033	6.463	6.902	0.993	37479

22

(a) $-10\sigma_{xz}$, $(\frac{5a}{12}, \frac{b}{2}, \bar{z})$ (b) $-10\sigma_{yz}$, $(\frac{a}{2}, \frac{5b}{12}, \bar{z})$
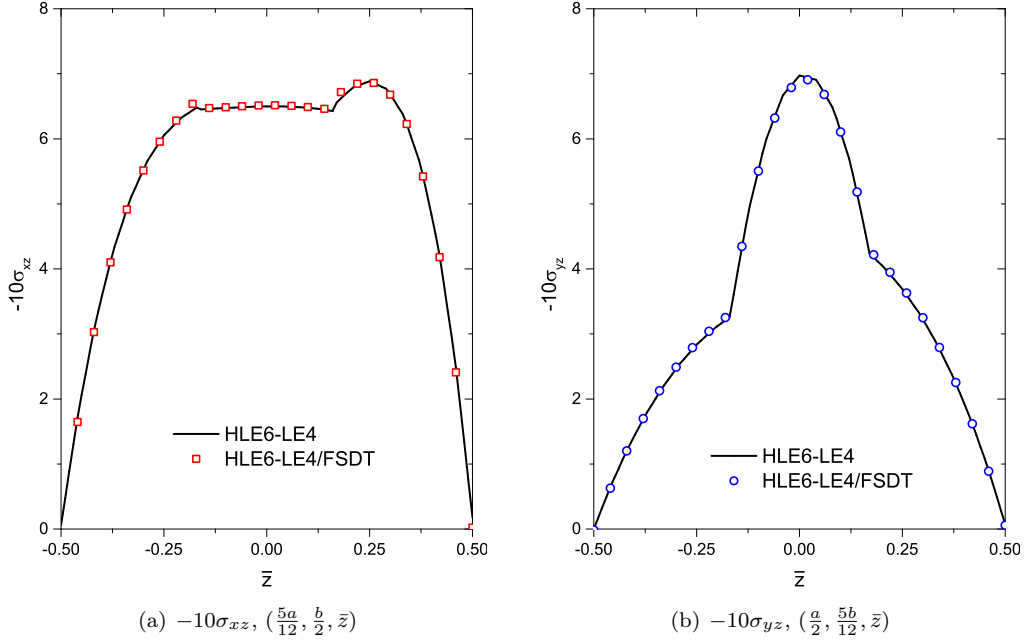
Figure 14: Variation of transverse shear stresses through $\bar{z}$ on the cross-ply composite plate under local pressure.

- The convergence rate of p-version refined 2D elements with higher-order Legendre polynomials as shape functions are better than h-refinement.

- With NDK, FE models with variable LW/ESL nodal kinematics can be conveniently constructed.

- By applying NDK, local kinematic refinement can be carried out without modifying the mesh neither using any artificial coupling method.

- NDK can help to further reduce the computational consumption when used together with Legendre-type plate elements for the analysis of structures undergoing strong local effects.

- The proposed approach is ideal for global-local analyses regarding both numerical efficiency and the convenience of modeling.

The proposed approach could also be extended to the modeling of laminated shells as future work.

23

10. Acknowledgment

References

[1] W. Koiter, On the foundations of the linear theory of thin elastic shell, Proc Kon Nederl Akad Wetensch 73 (3) (1970) 169–195.

[2] P. Naghdi, The theory of plates and shells, Handbuch der Physik, vol. VI a-2 (1972) 425–640.

[3] J. N. Reddy, A simple higher-order theory for laminated composite plates, Journal of Applied Mechanics 51 (4) (1984) 745–752.

[4] J. N. Reddy, Mechanics of laminated composite plates and shells: theory and analysis, CRC Press, 2004.

[5] A. N. Palazotto, Nonlinear analysis of shell structures, AIAA Series, 1992.

[6] E. Carrera, Theories and finite elements for multilayered, anisotropic, composite plates and shells, Archives of Computational Methods in Engineering 9 (2) (2002) 87–140.

[7] E. Carrera, M. Cinefra, M. Petrolo, E. Zappino, Finite element analysis of structures through Unified Formulation, John Wiley & Sons, 2014.

[8] M. Cinefra, S. Valvano, A variable kinematic doubly-curved MITC9 shell element for the analysis of laminated composites, Mechanics of Advanced Materials and Structures 23 (11) (2016) 1312–1325.

[9] E. Carrera, M. Cinefra, G. Li, G. Kulikov, MITC9 shell finite elements with miscellaneous through-the-thickness functions for the analysis of laminated structures, Composite Structures 154 (2016) 360–373.

[10] M. Cinefra, M. Petrolo, G. Li, E. Carrera, Hygrothermal analysis of multilayered composite plates by variable kinematic finite elements, Journal of Thermal Stresses 40 (12) (2017) 1502–1522. doi:10.1080/01495739.2017.1360164.

24

[11] M. Cinefra, M. Petrolo, G. Li, E. Carrera, Variable kinematic shell elements for composite laminates accounting for hygrothermal effects, Journal of Thermal Stresses 40 (12) (2017) 1523–1544. `doi:10.1080/01495739.2017.1360165`.

[12] E. Carrera, M. Cinefra, G. Li, Refined finite element solutions for anisotropic laminated plates, Composite Structures (2017) –`doi:dx.doi.org/10.1016/j.compstruct.2017.01.014`.

[13] R. E. Bank, The efficient implementation of local mesh refinement algorithms, Adaptive Computational Methods for Partial Differential Equations (1983) 74–81.

[14] J. Zhu, O. Zienkiewicz, Adaptive techniques in the finite element method, International Journal for Numerical Methods in Biomedical Engineering 4 (2) (1988) 197–204.

[15] B. Szabó, Some recent developments in finite element analysis, Computers & Mathematics with Applications 5 (2) (1979) 99–115.

[16] I. Babuška, B. A. Szabó, I. N. Katz, The p-version of the finite element method, SIAM Journal on Numerical Analysis 18 (3) (1981) 515–545.

[17] K. Surana, S. Petti, A. Ahmadi, J. Reddy, On p-version hierarchical interpolation functions for higher-order continuity finite element models, International Journal of Computational Engineering Science 2 (04) (2001) 653–673.

[18] B. Szabó, A. Düster, E. Rank, The p-Version of the Finite Element Method, Wiley Online Library, 2004.

[19] I. Babuška, B. Guo, The h-p version of the finite element method for domains with curved boundaries, SIAM Journal on Numerical Analysis 25 (4) (1988) 837–861.

[20] J. T. Oden, L. Demkowicz, W. Rachowicz, T. Westermann, Toward a universal hp adaptive finite element strategy, Part 2. A posteriori error estimation, Computer Methods in Applied Mechanics and Engineering 77 (1-2) (1989) 113–180.

[21] O. Zienkiewicz, J. Zhu, N. Gong, Effective and practical h–p-version adaptive analysis procedures for the finite element method, International Journal for Numerical Methods in Engineering 28 (4) (1989) 879–891.

[22] J. N. Reddy, An introduction to the finite element method, Vol. 2, McGraw-Hill New York, 1993.

[23] F. Brezzi, L. D. Marini, The three-field formulation for elasticity problems, GAMM-Mitteilungen 28 (2) (2005) 124–153.

[24] M. A. Aminpour, J. B. Ransom, S. L. McCleary, A coupled analysis method for structures with independently modelled finite element subdomains, International Journal for Numerical Methods in Engineering 38 (21) (1995) 3695–3718.

[25] W. Prager, Variational principles of linear elastostatics for discontinuous displacements, strains and stresses, Recent Progress in Applied Mechanics. The Folkey Odquist Volume. Stockholm: Almquist and Wiksell (1967) 463–474.

[26] P. Blanco, R. Feijóo, S. Urquiza, A variational approach for coupling kinematically incompatible structural models, Computer Methods in Applied Mechanics and Engineering 197 (17) (2008) 1577–1602.

[27] P. Blanco, P. Gervasio, A. Quarteroni, Extended variational formulation for heterogeneous partial differential equations, Computational Methods in Applied Mathematics 11 (2) (2011) 141–172.

[28] P. Blanco, R. Feijóo, Sensitivity analysis in kinematically incompatible models, Computer Methods in Applied Mechanics and Engineering 198 (41) (2009) 3287–3298.

[29] E. Carrera, A. Pagani, Analysis of reinforced and thin-walled structures by multi-line refined 1d/beam models, International Journal of Mechanical Sciences 75 (2013) 278–287.

[30] E. Carrera, A. Pagani, Multi-line enhanced beam model for the analysis of laminated composite structures, Composites Part B: Engineering 57 (2014) 112–119.

[31] H. B. Dhia, Multiscale mechanical problems: the Arlequin method, Comptes Rendus de l'Academie des Sciences Series IIB Mechanics Physics Astronomy 12 (326) (1998) 899–904.

[32] H. B. Dhia, G. Rateau, The Arlequin method as a flexible engineering design tool, International Journal for Numerical Methods in Engineering 62 (11) (2005) 1442–1462.

[33] F. Biscani, G. Giunta, S. Belouettar, E. Carrera, H. Hu, Variable kinematic plate elements coupled via Arlequin method, International Journal for Numerical Methods in Engineering 91 (12) (2012) 1264–1290.

26

[34] F. Biscani, P. Nali, S. Belouettar, E. Carrera, Coupling of hierarchical piezoelectric plate finite elements via Arlequin method, Journal of Intelligent Material Systems and Structures 23 (7) (2012) 749–764.

[35] J. Fish, The s-version of the finite element method, Computers & Structures 43 (3) (1992) 539–547.

[36] T. O. Williams, A generalized multilength scale nonlinear composite plate theory with delamination, International Journal of Solids and Structures 36 (20) (1999) 3015–3050.

[37] H. M. Mourad, T. O. Williams, F. L. Addessio, Finite element analysis of inelastic laminated plates using a global–local formulation with delamination, Computer Methods in Applied Mechanics and Engineering 198 (3) (2008) 542–554.

[38] D. Versino, H. M. Mourad, T. O. Williams, A global–local discontinuous galerkin shell finite element for small-deformation analysis of multi-layered composites, Computer Methods in Applied Mechanics and Engineering 271 (2014) 269–295.

[39] D. Versino, H. M. Mourad, T. O. Williams, F. L. Addessio, A global–local discontinuous galerkin finite element for finite-deformation analysis of multilayered shells, Computer Methods in Applied Mechanics and Engineering 283 (2015) 1401–1424.

[40] E. Carrera, E. Zappino, One-dimensional finite element formulation with node-dependent kinematics, Computers & Structures 192 (2017) 114–125.

[41] E. Carrera, E. Zappino, G. Li, Finite element models with node-dependent kinematics for the analysis of composite beam structures, Composites Part B: Engineering 132 (Supplement C) (2018) 35 – 48.

[42] E. Carrera, A. Pagani, S. Valvano, Multilayered plate elements accounting for refined theories and node-dependent kinematics, Composites Part B: Engineering 114 (2017) 189–210.

[43] E. Zappino, G. Li, A. Pagani, E. Carrera, Global-local analysis of laminated plates by node-dependent kinematic finite elements with variable ESL/LW capabilities, Composite Structures 172 (2017) 1–14.

[44] S. Valvano, E. Carrera, Multilayered plate elements with node-dependent kinematics for the analysis of composite and sandwich structures, FACTA UNIVERSITATIS. SERIES: MECHANICAL ENGINEERING 15 (1) (2017) 1–30.

27

[45] E. Carrera, S. Valvano, G. M. Kulikov, Multilayered plate elements with node-dependent kinematics for electro-mechanical problems, International Journal of Smart and Nano Materials 0 (0) (2017) 1–39. `doi:10.1080/19475411.2017.1376722`.

[46] E. Carrera, E. Zappino, G. Li, Analysis of beams with piezo-patches by node-dependent kinematic finite element method models, Journal of Intelligent Material Systems and Structures 0 (0) (0) 1045389X17733332. `doi:10.1177/1045389X17733332`.

[47] B. A. Szabó, I. Babuška, Finite element analysis, John Wiley & Sons, 1991.

[48] A. Peano, Hierarchies of conforming finite elements for plane elasticity and plate bending, Computers & Mathematics with Applications 2 (3-4) (1976) 211–224.

[49] B. Szabó, A. Mehta, p-convergent finite element approximations in fracture mechanics, International Journal for Numerical Methods in Engineering 12 (3) (1978) 551–560.

[50] O. C. Zienkiewicz, J. D. S. Gago, D. W. Kelly, The hierarchical concept in finite element analysis, Computers & structures 16 (1) (1983) 53–65.

[51] A. Pagani, A. de Miguel, M. Petrolo, E. Carrera, Analysis of laminated beams via Unified Formulation and Legendre polynomial expansions, Composite Structures 156 (2016) 78 – 92, 70th Anniversary of Professor J. N. Reddy.

[52] E. Carrera, A. de Miguel, A. Pagani, Hierarchical theories of structures based on Legendre polynomial expansions with finite element applications, International Journal of Mechanical Sciences 120 (2017) 286–300.

[53] N. J. Pagano, Exact solutions for rectangular bidirectional composites and sandwich plates, Journal of Composite Materials 4 (1) (1970) 20–34.

[54] G. Kulikov, S. Plotnikova, Exact 3D stress analysis of laminated composite plates by sampling surfaces method, Composite Structures 94 (12) (2012) 3654–3663.

[55] E. Carrera, A. Ciuffreda, Bending of composites and sandwich plates subjected to localized lateral loadings: a comparison of various theories, Composite Structures 68 (2) (2005) 185–202.